Journal of Solid State Chemistry 186 (2012) 36–46

Contents lists available at SciVerse ScienceDirect

Journal of Solid State Chemistry

journal homepage: www.elsevier.com/locate/jssc

Thermochemical and kinetic aspects of the sulfurization of Cu–Sb and Cu–Bi thin films

Diego Colombara [a,*], Laurence M. Peter [a], Keith D. Rogers [b], Kyle Hutchings [b]

[a] Department of Chemistry, University of Bath, Bath BA2 7AY, UK
[b] Centre for Materials Science and Engineering, Cranfield University, Shrivenham, SN6 8LA, UK

ARTICLE INFO

Article history:
Received 14 September 2011
Received in revised form
26 October 2011
Accepted 15 November 2011
Available online 28 November 2011

Keywords:
Photovoltaics
Sulfurization
RTP
Phase evolution
Pilling–Bedworth
Hydrogen sulfide

ABSTRACT

$CuSbS_2$ and Cu_3BiS_3 are being investigated as part of a search for new absorber materials for photovoltaic devices. Thin films of these chalcogenides were produced by conversion of stacked and co-electroplated metal precursor layers in the presence of elemental sulfur vapour. Ex-situ XRD and SEM/EDS analyses of the processed samples were employed to study the reaction sequence with the aim of achieving compact layer morphologies. A new "Time-Temperature-Reaction" (TTR) diagram and modified Pilling–Bedworth coefficients have been introduced for the description and interpretation of the reaction kinetics. For equal processing times, the minimum temperature required for $CuSbS_2$ to appear is substantially lower than for Cu_3BiS_3, suggesting that interdiffusion across the interfaces between the binary sulfides is a key step in the formation of the ternary compounds. The effects of the heating rate and sulfur partial pressure on the phase evolution as well as the potential losses of Sb and Bi during the processes have been investigated experimentally and the results related to the equilibrium pressure diagrams obtained via thermochemical computation.

1. Introduction

In many fields of materials science such as thin film photovoltaics, fuel cells, batteries and protective coatings, the compound of interest is often formed via reaction of a solid precursor with gaseous or liquid species. Examples are the preparation of copper indium (gallium) diselenide (CI(G)S) and copper zinc tin siulfide (CZTS) absorber layers for thin film solar cells [1–3], $LiCo(Ni)O_2$ cathodes for molten carbonate fuel cells and lithium-ion batteries [4,5] and the formation of protective barriers by passivation treatments of precursor coatings [6].

The reaction chemistries involved in film formation are generally complex, but in most cases there appears to be a competition between the rates of reaction and mass transfer [7]. For example, in the case of chalcogenisation of metal binary or ternary precursors, a large number of intermetallic alloys may form over the processing timescale. Although the final products of the process can be reasonably deduced from the equilibrium phase diagrams (if these are available), the morphology of the resulting film is often driven by the reaction trajectory and associated phase segregations.

The present study is part of a broader research project aimed at investigating economically-viable alternatives to CI(G)S as *p*-type materials for photovoltaic applications. Previous studies [8,9] have shown that $CuSbS_2$ and Cu_3BiS_3 are photoactive *p*-type semiconductors with band-gaps that are suitable for photovoltaic (PV) applications. However, preparative aspects such as secondary phase segregation, compositional stability and film morphology require optimisation. It follows that a deeper understanding of the thermodynamics and kinetics of sulfurization reaction is, therefore, of crucial importance.

In the present work, the phase evolution of Cu:Sb 1:1 and Cu:Bi 3:1 metal precursor films (layered or homogeneous configuration) during sulfurization with either elemental sulfur vapour or hydrogen sulfide was analyzed critically in order to elucidate the roles of diffusion and phase equilibria in the kinetics of compound formation, film morphology and potential loss of elements during the thermal processes. The study has highlighted the utility of thermochemistry in the prediction of such phenomena. The approach developed here should find application to other materials systems.

2. Experimental details

Precursor films of Cu:Sb 1:1 and Cu:Bi 3:1 were obtained by electrodeposition from aqueous solutions onto Mo coated glass substrates as described elsewhere [8]. Two configurations were employed; stacked and co-electroplated. The precursor film thickness was chosen so that the corresponding sulfide layers would be 2 μm thick.

* Corresponding author.
E-mail address: dc326@bath.ac.uk (D. Colombara).

0022-4596/$ - see front matter © 2011 Elsevier Inc. All rights reserved.
doi:10.1016/j.jssc.2011.11.025

The conversion of the metal precursor films into the corresponding sulfides was performed within graphite boxes in the presence of elemental sulfur vapour either in an AS-Micro Rapid Thermal Processor (AnnealSys) or in a wire-wound quartz tubular furnace (Thermo Scientific). The following sulfurization parameters were investigated: temperature (ranging between 200 and 550 °C), dwell period (between 5 and 960 min), and heating rate (between 5 and 600 °C min^{-1}).

The phase evolution study was performed by analyzing the ex-situ X-ray diffractograms of quenched samples, as reported in earlier work [8]. Morphological and compositional analyses were performed with a Jeol 6480LV SEM connected to an INCA x-act EDS microprobe.

3. Results and discussion

3.1. Reaction sequence via structural characterization

The phase evolution of the Cu–Sb and Cu–Bi films as a function of the sulfurization temperature is illustrated by Fig. 1a–b, where the integrated intensity of the relevant ex-situ XRD reflections of the phases involved are plotted for samples sulfurized at a given temperature for 5 min and for 30 min. Such plots are not intended as quantitative estimations, since the absolute magnitudes are not necessarily significant. However, the changes in relative intensities for each phase provide a valid picture of the evolution of the different species. Although there are minor structural differences between stacked and co-deposited precursors [8,9], the phase evolution profiles obtained in this way were found to be similar for both precursor configurations (ref. to supporting information).

The contribution of each phase and reflections are considered as follows:

(a) Sb PDF no 35–732 [(0 0 3)+(0 0 6)+(0 0 9)], CuS PDF no 65–3561 [(0 0 6)], Sb_2S_3 PDF no 42–1393 [(2 0 0)+(0 2 0)+(1 2 0)+(4 1 2)+(2 1 4)+(5 0 2)+(2 0 5)], $CuSbS_2$ PDF no 65–2416 [(1 0 2)+(0 1 5)+(2 1 3)+(0 1 7)+(0 1 8)].
(b) Bi (black) PDF no 44–1246 [(0 1 2)+(1 0 4)], CuS PDF no 65–3561 [(1 0 1)+(1 0 2)], Bi_2S_3 PDF no 6–333 [(1 2 1)+(2 3 0)+(1 3 0)+(3 1 0)], Cu_3BiS_3 PDF no 9–488 [(1 1 1)+(2 0 0)+(0 1 2)+(2 2 0)+(1 1 2)+(1 3 0)+(0 4 0)].

The colour of the films was found to relate to the composition observable by XRD: films rich in CuS were blue, whereas films composed predominantly of the ternary sulfide ($CuSbS_2$ or Cu_3BiS_3) were gray. No colour difference was noticed between the samples of the two configurations sulfurized at the same temperature. This suggests that the configuration of the metal precursors (stacked or co-electroplated) seems to have little influence on the phase evolution vs temperature. However, more detailed investigations are required to fully examine this specific aspect.

Fig. 1 suggests that the systems follow a sequential reaction/diffusion mechanism, where the metals react selectively with sulfur to form the corresponding sulfides. The ternary compounds then emerge as diffusion products from the binaries when the temperature is sufficiently high or the dwell time is sufficiently long. The two reaction sequences that this implies are:

(1) $2Cu_{(s)}+S_{2(g)}\rightarrow 2CuS_{(s)}$
(2) $4Sb_{(s)}+3S_{2(g)}\rightarrow 2Sb_2S_{3(s)}$
(3) $4CuS_{(s)}+2Sb_2S_{3(s)}\rightarrow 4CuSbS_{2(s)}+S_{2(g)}$

(1) $2Cu_{(s)}+S_{2(g)}\rightarrow 2CuS_{(s)}$
(4) $4Bi_{(s)}+3S_{2(g)}\rightarrow 2Bi_2S_{3(s)}$
(5) $12CuS_{(s)}+2Bi_2S_{3(s)}\rightarrow 4Cu_3BiS_{3(s)}+3S_{2(g)}$

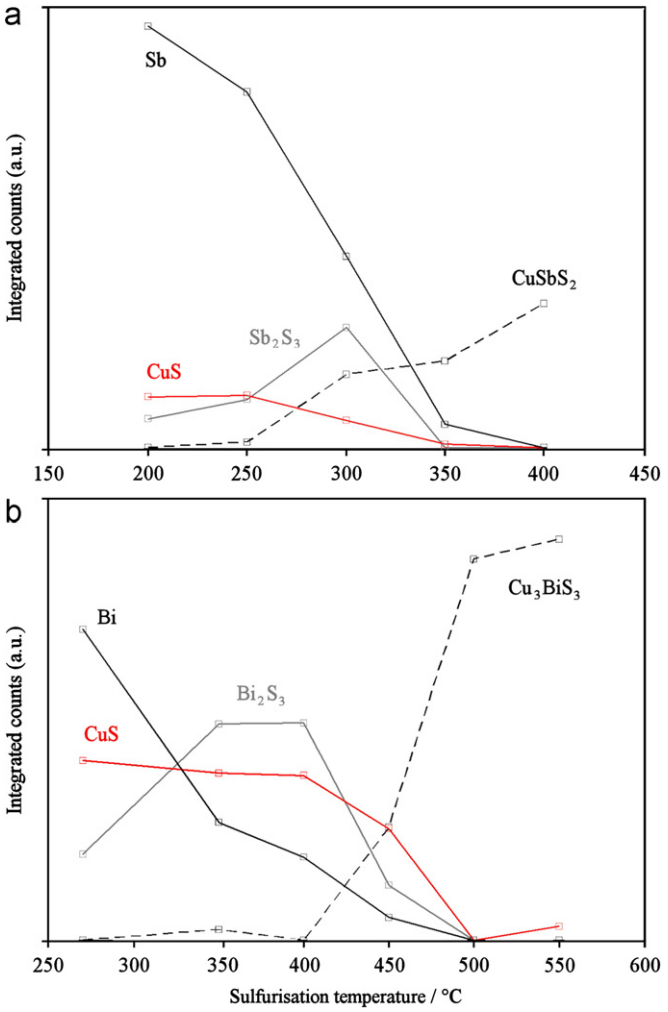

Fig. 1. Ex-situ XRD integrated peak intensities for Cu:Sb=1:1 stacked (a) and Cu:Bi=3:1 codeposited (b) precursor films after sulfurization treatments lasting 30 and 5 min respectively.

Cu seems to be consumed rather quickly, since no traces of its XRD peaks are observable at any of the sulfurization temperatures investigated. The integrated XRD peaks corresponding to CuS remain more or less constant until the sulfurization temperature is sufficiently high to allow formation of the ternary sulfides (300 °C for $CuSbS_2$ and 450 °C for Cu_3BiS_3) at which point the peak counts start to decrease. This suggests that all of the Cu is promptly available as CuS for the subsequent formation of the ternary compounds, even at temperatures as low as 200 °C. By contrast, the XRD peaks corresponding to elemental Sb and Bi (M) remain clearly visible up to 350 and 450 °C respectively, suggesting that sulfur uptake by these elements is more sluggish. Over the range of dwell times considered, M_2S_3 coexists with M and CuS until the conversion to the ternary sulfide comes to an end. The trend of the corresponding XRD peak counts versus temperature exhibits a maximum corresponding to the temperature at which the rate of M_2S_3 formation equals its rate of consumption in the reactions forming $CuSbS_2$ and Cu_3BiS_3.

The build up and subsequent decay of the binary sulfides suggests that the rate determining step for the formation of the ternary compounds is the solid state diffusion of the elements across their interfaces. If this was not true, the binary phases would not be detected along with the ternaries (Fig. 1). It should be noted that the plots in Fig. 1a–b are typical for dwell periods

of 30 and 5 min respectively, i.e. they both represent "out-of-equilibrium" conditions, where the samples under reaction have been "quenched" and their phase composition at each temperature can be assumed to be frozen. Ideally, one would have to perform temperature resolved in-situ isothermal monitoring, in order to create a complete time-temperature reaction (TTR) diagram, in a similar fashion to the common time-temperature transformation (TTT) diagrams that are widely employed to represent the transformation kinetics in metallurgy and other fields. Similarly to the TTT, such TTR diagrams are only valid for describing the phase composition of the samples at ideally fixed precursor film configuration, thickness, and sulfurizing conditions (sulfur source and its partial pressure). The morphology of the phases will, in principle, depend on the reaction pathway followed during the treatment.

Since our findings indicated that higher temperatures were required to convert the Cu–Bi samples to Cu_3BiS_3 in the presence of sulfur vapour compared to the work by Haber et al. [10], who used H_2S, an attempt was made to produce a TTR diagram for the formation of Cu_3BiS_3 from the co-electroplated (i.e. homogeneous [9]) Cu:Bi 3:1 metal precursors and elemental sulfur vapour. This allows a sound comparison of the two sulfurization techniques. The thermal treatments were prolonged up to 16 h at 270 and 350 °C, in order to ascertain the minimum temperature required for Cu_3BiS_3 to form under "close-to-equilibrium" conditions. The result is shown in Fig. 2.

The two lines in Fig. 2 divide the time-temperature plot into three regions representing three different phase compositions. In region (a) the phases present are $Bi_{(s)}$, $Bi_2S_{3(s)}$ and $CuS_{(s)}$, in region (b) $Cu_3BiS_{3(s)}$ starts to appear and in region (c) the reaction is complete and the solid system is monophasic (unless excess binary phases are present due to non stoichiometry of the precursors).

For processing time up to 16 h it was found that the reaction is largely incomplete at 350 °C, while at 270 °C ternary sulfide formation does not occur at all. Clearly, longer dwell periods would be necessary in order to complete the diagram in the lower temperature range. Indeed, if nucleation and growth of the ternary phase becomes impossible due to either thermochemical or kinetic

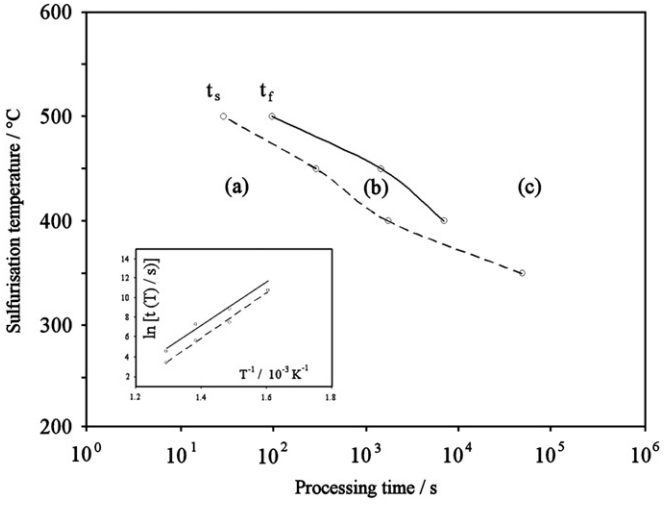

Fig. 2. Time Temperature Reaction (TTR) diagram for the conversion of co-electroplated Cu:Bi 3:1 metal precursor into 2 μm thick Cu_3BiS_3 layer in the presence of elemental sulfur vapour at a partial pressure of 500 mbar. The plot was created by ex-situ XRD analysis of rapid thermal processed samples (600 °C min^{-1}) after quenching. The dashed line represents the emergence of the ternary sulfide (t_s) and the solid line the reaction completion (t_f). Inset: modified Arrhenius plot for the estimation of the activation energy of Cu_3BiS_3 formation.

reasons, the limiting situation could well correspond to t_s and t_f lines parallel or quasi-parallel to the abscissa, representing processing times approaching infinity at a critical temperature.

The formation of intermediate sulfide phases in the solid state from the binaries has been studied by Ross [11] via observation of the phase evolution in bulk diffusion couples. The rates of intermediate phase formation in the Cu_2S–Sb_2S_3 system were observed to obey Tammann's parabolic rate rule for diffusion [12,13]

$$x = [2k(T)\cdot t]^{1/2} \quad (1)$$

where x is the thickness of the developing intermediate phase, $k(T)$ is the rate constant and t is the time.

Ross developed a theoretical model for the kinetics based on the simultaneous and chemically-equivalent interchange of the two kinds of metal ions, migrating in opposite direction through the sulfur network of the emerging phase.

Assuming that the CuS–Bi_2S_3 system follows a similar behaviour, information on the kinetics of Cu_3BiS_3 phase formation can be extracted from the data in the TTR diagram.

The temperature dependence of the reaction rate constant is given by the Arrhenius equation,

$$k(T) = A\cdot e^{-E_a/RT} \quad (2)$$

where A is a pre-exponential factor, E_a is the activation energy of the reaction, R is the universal gas constant and T is the absolute temperature. By substituting Eq. (2) in Eq. (1), one can estimate the activation energy for ternary sulfide formation in thin films by analyzing the temperature dependence of the time required for the relevant phase to form, Eq. (3).

$$\ln[t_{s,f}] = \ln(x^2/2A) + (E_a/RT) \quad (3)$$

A plot of $\ln[t_{s,f}]$ versus $1/T$ will give a straight line, with a slope equals to E_a/R (Fig. 2, inset).

Due to the geometry of our system (thin films), the measurement of the thickness of the developing phase is hard to achieve, but nevertheless useful kinetic information can be extracted from the temperature dependence of the time required for the phase to emerge (t_s) and form completely (t_f). If the assumptions regarding diffusion are correct, precursors with different thicknesses will give rise to lines that are shifted on the y-axis, but with the same slope. A similar behaviour is expected if binary sulfide segregation is altered, either because of a different precursor configuration or especially due to different sulfurization conditions. This would affect the contact area of the reacting species leading to a variation of the pre-exponential factor in the Arrhenius equation.

A value of $\sim$180 kJ mol^{-1} was estimated as the average activation energy for the formation of Cu_3BiS_3 thin films from CuS and Bi_2S_3. By comparison, the reported [11] activation energy for the formation of bulk $CuSbS_2$ from Cu_2S and Sb_2S_3 is much lower, $\sim$33 kj mol^{-1}.

This is consistent with the observation that for the Cu–Bi system at 350 °C, the ternary compound appears only after very long time (16 h). In the case of the Cu–Sb system at the same temperature, $CuSbS_2$ is completely formed, after a dwell period as short as 30 min [8].

Similarly, comparison of the series of XRD analyses of sulfurized evaporated Sb [8] and Bi films [9] suggests a more sluggish reaction of Bi with sulfur compared to Sb.

Bi_2S_3 (*Bismuthinite*) and Sb_2S_3 (*Stibnite*) are isostructural compounds [14] with the group-five element in the trivalent state. Their structure is characterised by tightly-bonded M_4S_6 rods displaced in a herring bone arrangement [15], with pronounced steric requirements of the lone electron pairs accommodated between the rods [16]. The effective ionic radii [17] of Bi in trivalent form are on average about 36% larger than those of Sb

[18], which is likely to lead to more sluggish diffusion of Bi through the M_2S_3/CuS crystallite interface, and to a higher value of the activation energy for the compound formation.

As already pointed out in our previous work [9], our results differ substantially from those reported by Haber et al. [10] in terms of phase evolution versus temperature, as no evidence of Cu_3BiS_3 was identified in the time frame of 16 h at 270 °C, and even at 350 °C the reaction is largely incomplete.

In the modified Arrhenius plot, the increase in slope of the lines corresponding to t_s and t_f is an indication of higher activation energy for nucleation and growth of the ternary phase. This is consistent with either a different diffusion mechanism, or with a change of the sign of the Gibbs free energy of reaction (5) in the low temperature regime.

In this context a different sulfur source and pressure would likely affect the shape of the TTR diagram due to both mass action (cf. reaction (5)) and to a change in the kinetics of binary sulfides formation.

In fact, in our case elemental sulfur vapour was employed as sulfurizing agent (~500 mbar at 270 °C during the first stages of the sulfurization treatment, slowly decreasing to a minimum pressure of ~23 mbar owing to $S_{2(g)}$ diffusion out of the graphite susceptor), while H_2S was used by Haber et al. [10] (~7 mbar).

The role of the sulfurizing conditions on the phase evolution of the systems is considered in Section 3.3.

3.2. Morphological implications of the reaction sequence

The EDS/SEM analyses of the Cu–Sb and Cu–Bi sulfurized samples presented in our previous papers [8,9] show that the formation of the binary sulfides is accompanied by phase segregation, prior to the development of the ternary compound. Fig. 3 illustrates the top and

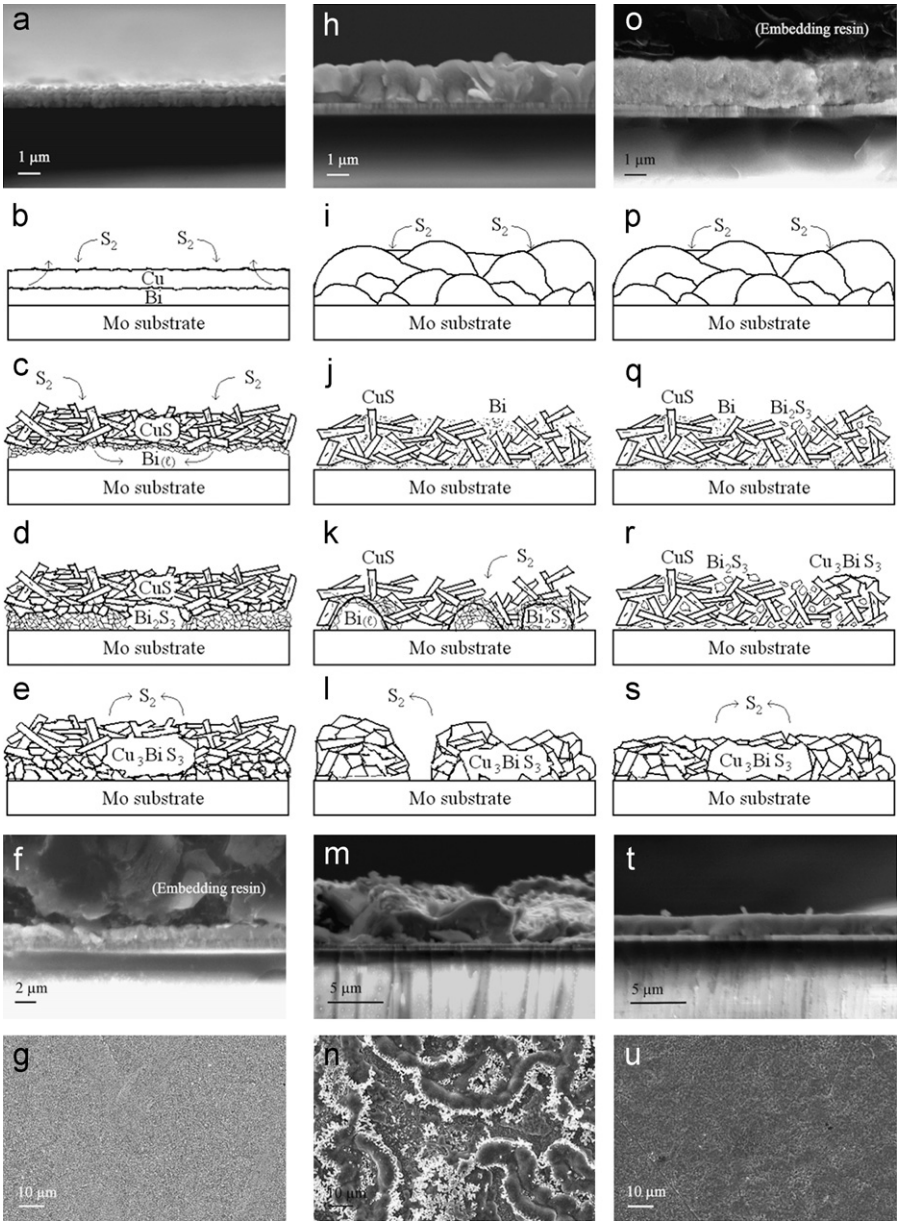

Fig. 3. Phase evolution model for the interpretation of the structural and morphological results of the sulfurization of stacked (a) and co-electroplated (h,o) Cu:Bi 3:1 metal precursor films in the presence of elemental sulfur vapour with heating rates of 600 °C min^{-1} (b–e, i–l) and 5 °C min^{-1} (p–s); the corresponding SEM cross sectional (f,m,t) and top views (g,n,u) are included.

cross sectional morphologies of the Cu:Bi 3:1 stacked and co-electroplated metal precursors before (a,h,o) and after sulfurization treatments with heating rates of 600 (f–g, m–n) and 5 °C min^{-1} (t–u). The strikingly different behaviours of the stacked (a–g) and co-electroplated precursors (h–n) under sulfurization at fast heating rate as well as of the co-electroplated precursor under fast (h–n) and slow heating rates (o–u) are meaningful. The structural findings reported in Section 3.1 reveal that all of the Cu is promptly converted to CuS at temperatures as low as 200 °C. A phase evolution model that fits all these results is proposed in Fig. 3.

Crystallites of CuS segregate at the surface of the former precursor film [8,9], meaning that the unreacted Bi is left underneath (Fig. 3c) or dispersed amongst the CuS crystals (Fig. 3j–q). Once the temperature is higher than ~270 °C the unreacted Bi melts and, in the case of the co-electroplated precursor, it segregates from the rest in a "dewdrop" fashion (Fig. 3k). The remaining Bi is then slowly converted to Bi_2S_3 and the ternary sulfide starts to appear at the interface between the binaries.

Very low heating rates must be employed to achieve a good film morphology using the homogenous Cu–Bi co-electroplated precursor. Under these conditions, the conversion of Bi into Bi_2S_3 occurs before the temperature reaches the melting point of the element. This avoids the formation of the liquid framework (Fig. 3r) and leads to samples of improved morphology (Fig. 3s–u) [9].

The poor morphology and adhesion (Fig. 3m–n) of the co-electroplated Cu–Bi films sulfurized at temperatures higher than ~270 °C with heating rates exceeding 5 °C min^{-1} were already indicated in previous investigations [9]. In our work, localised EDS analysis and EDS mapping show the presence of Cu, Bi and S in the remaining parts of the film, while just Mo and S are detected on a large fraction of the sample area (Fig. 4c–e). The smooth edges of the residual film suggest that it has undergone partial melting and coalescence, with consequential exposure of the underlying Mo layer.

As can be seen in Fig. 3f–g, this phenomenon is not observed if the Cu–Bi precursor employed is in a stacked configuration. In this case all of the Bi is already in contact forming a compact metal film prior to its melting.

As reported elsewhere [9], the XRD analysis of the as-deposited and annealed (without sulfur) co-electroplated Cu–Bi film suggests that Bi is homogeneously intermixed with Cu in the precursor and a rise in temperature causes the two elements to separate forming detached aggregates.

The morphological peculiarity of the co-electroplated Cu–Bi films sulfurized with high heating rate can be explained on the basis of the Bi–Cu phase equilibria [21]. The binary phase diagram (Fig. 4f) shows negligible mutual solubility of the end members in the solid state with no other intermediate compounds, and the

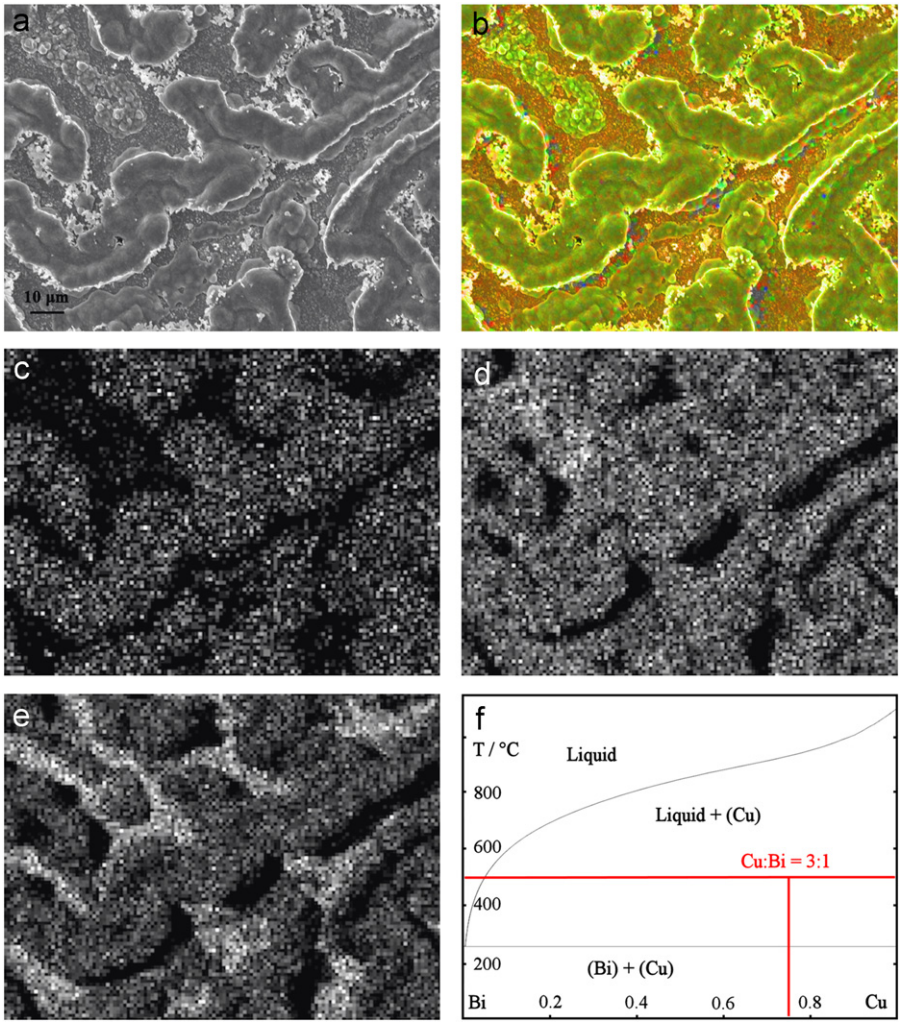

Fig. 4. (a) Secondary electron micrograph of a co-electroplated Cu:Bi 3:1 precursor sample sulfurized at 500 °C for 5 min (heating rate employed: 600 °C min^{-1}); (b) overlaying of (a) with X-ray signals chromatically depicted in the range 2.2 ÷ 3.0 keV including L_α, K_α and M_α lines of Mo, S and Bi respectively. EDS maps of (a) relative to: K_α line of Cu (c), M_α line of Bi (d) and L_α and K_α lines of Mo and S (e). (f) Adapted Bi–Cu equilibrium phase diagram calculated using MTDATA, software from the National Physical Laboratory for the calculation of phase equilibria from thermodynamic data [19] (original data taken from [20]).

presence of a eutectic transformation at 270.6 °C (just below the melting temperature of pure Bi, 271.4 °C) with composition 99.5% at. Bi.

Given the initial composition of the electrodeposit (~25% at. Bi) and the mentioned phase equilibria, it can be estimated that ~25% at. of the homogenous precursor will form a liquid (with composition ~98.5% at. Bi) at the eutectic temperature. Due to the steepness of the liquidus boundary, a further increase of the temperature up to 500 °C will cause only a limited additional part (~1.3% at.) of the precursor to melt to form a liquid of slightly increased Cu concentration (~95% at. Bi). This means that at the eutectic temperature the large majority of the Bi initially dispersed in the deposit separates from the homogenous precursor to form a liquid that tends to coalesce to minimise the surface tension.

According to our findings, the morphology of the final Cu_3BiS_3 film is driven by the development and displacement of the phases during the sulfurization treatments, leading to films of reasonably good consistency (Fig. 3e–g, s–u) or poor continuity (Fig. 3l–n) depending on the precursor configurations and heating rates utilized.

According to the results of the present study, the introduction of sulfur into homogeneous rather than stacked metal precursors does not seem to involve a simpler diffusion mechanism as had been thought previously [8]. Conversely, phase segregation during treatment was shown to be even more pronounced for the Cu–Bi co-electroplated precursor, if high heating rates were employed.

The different reactivity of the metallic elements towards the sulfur source has a strong role on the phase evolution within the systems. These aspects are addressed in more detail in Section 3.3.

3.3. Role of the sulfurizing conditions on the phase evolution

It seems clear that the nature and amounts of the reacting species employed in the atmosphere play a major part in the fate of the precursor. Consequently, the behaviours of $S_{2(g)}$ and $H_2S_{(g)}$ as reagents for the sulfurization of metallic Cu, Bi, and Sb have been investigated from a thermochemical standpoint. The approach involves plotting the temperature dependence of the Gibbs free energies of the relevant reactions, normalised per one mole of metal for the sake of comparison (Fig. 5). The calculations were based on the thermochemical data by Knacke et al. [22].

(1) $2Cu_{(s)}+S_{2(g)}\rightarrow 2CuS_{(s)}$
(1b) $2Cu_{(s)}+2H_2S_{(g)}\rightarrow 2CuS_{(s)}+2H_{2(g)}$
(2) $4Sb_{(s,l)}+3S_{2(g)}\rightarrow 2Sb_2S_{3(s)}$
(2b) $4Sb_{(s,l)}+6H_2S_{(g)}\rightarrow 2Sb_2S_{3(s)}+6H_{2(g)}$
(4) $4Bi_{(s,l)}+3S_{2(g)}\rightarrow 2Bi_2S_{3(s)}$
(4b) $4Bi_{(s,l)}+6H_2S_{(g)}\rightarrow 2Bi_2S_{3(s)}+6H_{2(g)}$

As discussed by Berg et al. [23], the sulfur vapour is mostly composed of $S_{8(g)}$–$S_{6(g)}$ rings up ~620 °C, whereas the $S_{2(g)}$ species becomes predominant at higher temperature. Therefore the thermodynamic calculation was based on the data for the most stable molecular sulfur species at each temperature.

From the trends in Fig. 5 it is clear that the sulfurizations via $H_2S_{(g)}$ (dashed lines) have a smaller driving force than the corresponding reactions involving $S_{n(g)}$ (solid lines). This general rule of thumb seems to agree with the weaker nucleation and larger grain size reported when sulfurizations of other systems are performed in hydrogen sulfide as opposed to elemental sulfur vapour under similar conditions [24]. Also, the positive slope of the lines seems to correlate well with the increasing grain size generally observed when the effect of the increase of sulfurization temperature is investigated by the rapid thermal process approach [25,26].

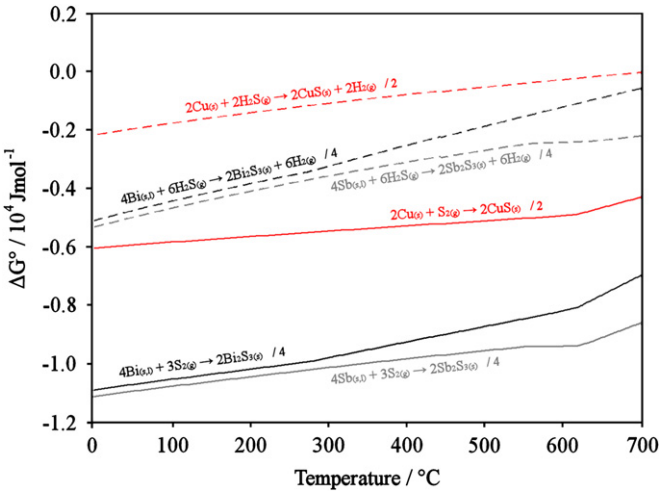

Fig. 5. Temperature dependence of the standard Gibbs free energies of sulfurization for Cu, Bi, and Sb with $S_{2(g)}$ (solid lines) and $H_2S_{(g)}$ (dashed lines).

It is interesting to notice that, based on the ΔG° values, the driving forces for sulfurizations of Cu via both $H_2S_{(g)}$ and $S_{2(g)}$, are lower than for the corresponding reactions of Bi and Sb. The experimental evidence of a more prompt reaction of Cu with $S_{2(g)}$ as opposed to Bi and Sb [8], therefore has to be explained on the basis of kinetics.

The ΔG values for sulfurization of Bi and Sb in both $H_2S_{(g)}$ and $S_{2(g)}$ show a very similar trend, with the driving force for Bi sulfurization being slightly lower than for Sb. This ties in with the more sluggish reaction of Bi compared to Sb [8], which suggests that the sulfurization of these two metals might be hindered by the same kinetic reasons (remember that Bi_2S_3 (*Bismuthinite*) and Sb_2S_3 (*Stibnite*) are isostructural compounds [14]).

The nucleation and growth of CuS on the surface of Cu is such that the underlying metal is easily exposed to the reacting atmosphere [9]. By contrast, electrochemical anodisation of Sb and Bi give rise to adherent sulfide films on the surface of unreacted metal [27,28].

The concept of the Pilling–Bedworth ratio (R_{PB}) [29] can be borrowed from corrosion science and oxide formation as a qualitative indicator of the structural compatibility between a metal and its own sulfide growing onto its surface. For a generic metal sulfide of formula M_xS_y, the modified Pilling–Bedworth ratio is given by Eq. (4):

$$R_{PB} = V_{M_xS_y}/xV_M = \rho_M W_{M_xS_y}/x\rho_{M_xS_y} W_M \quad (4)$$

where R_{PB} is the adapted Pilling–Bedworth ratio, while V, ρ and W are the molar volume (mol cm^{-3}), the density (g cm^{-3}) and the molar mass (g mol^{-1}) respectively of the metal (M) and its sulfide (M_xS_y).

If this ratio is less than 1, the volume of the sulfide formed is less than that of the metal which it replaces so that the sulfide film will be under expansion strain and it will ultimately crack to form a cellular, porous structure. If the opposite is true, a continuous enveloping film of sulfide should form which is free to expand outwards; this isolates the surface of the underlying metal from free contact with the sulfur atmosphere, delaying the conversion completion. However, if the ratio is too high, the sulfide layer may flake off due to excess compression strains. This is just a general rule of thumb, since it does not take into account other properties of the species involved. Clearly, the process conditions, as well as the sulfurizing agent and partial pressure

employed will have an effect on the nucleation formation and on possible preferential directions of growth.

Computation of the Pilling–Bedworth ratio for the interfaces relevant to our study gives the following results, which seem to agree with the relative reactivity of the elements considered: 2.87 for Cu/CuS, 2.02 for Sb/Sb_2S_3 and 1.77 for Bi/Bi_2S_3. Among the three cases, Cu/CuS has the highest R_{PB}, and this would explain the prompt sulfurization of copper. Conversely, the Bi/Bi_2S_3 has a particularly low value of R_{PB} (>1), making Bi_2S_3 a physical hindrance for the conversion reaction.

This explanation seems to agree with the findings of Haber et al. [10], who observed that the rate of formation of Cu_3BiS_3 at 270 °C is increased if Bi_2S_3 is already present in the precursor film (CuS–Bi co-sputtering was employed), in which case Bi_2S_3 is available straightaway for the compound formation and there is no need for the sulfur uptake of Bi to occur. Besides this, it is known that Cu in the non stoichiometric phases $Cu_{2-x}S$ with x up to 0.066 shows exceptionally high mobility, due to a mechanism based on vacancy exchange [30,31]. Sulfurization of homogenous bulk brass samples also occurs with selective reaction of Cu and sulfur, to form a Cu_2S layer that grows via outward cation migration accompanied by the appearance of pores localized at the alloy/Cu_2S interface [32]. Similar kinetics of sulfide growth has been reported to occur under conditions where covellite (CuS) forms on the surface of bulk Cu [33] and it is likely to be the case also for the present study.

During electrochemical anodisation of Cu electrodes, thin films of Cu_2S are formed first, followed by CuS growth with anodic charge/time profile typical for a control of the process via diffusion of Cu ions through the growing film [34,35]. On the other hand, a recent electrochemical impedance spectroscopy model is based on the assumption that anodic Bi_2S_3 grows via transport of anion (sulfide) vacancies [36].

The larger ΔG° of sulfurization of Cu with elemental sulfur vapour, as opposed to hydrogen sulfide, is thought to be the main reason for the delay in the formation of Cu_3BiS_3 in the present case, compared to the work by Haber et al. [10]. We believe that the stronger thermodynamic driving force, enhanced by a higher partial pressure of the sulfurizing reagent, causes the Cu to react fairly quickly, forming segregated CuS at the surface of the former precursor film. If the sulfur vapour is replaced by hydrogen sulfide, the sulfurization reaction is slower (probably also for kinetic reasons), and it occurs on a time scale that is more similar to the sulfurization of Bi. Gerein et al. have shown that sulfur incorporation from H_2S leads to amorphous copper sulfide at lower temperatures (300 °C) [37] and to $Cu_{2-x}S$ at higher temperatures [10]. In the first case lateral segregation of the binary phases is reduced and inter-diffusion of Cu and Bi is facilitated. In the second case the reaction with Bi_2S_3 would occur with less thermochemical and kinetic hindrances, due to the reduced amount of evolving sulfur (cf. reaction (5)).

Higher temperatures (or longer times) are indeed required, in the present work, in order to compensate for the reduced CuS/Bi_2S_3 contact area (arising from segregation of CuS at the surface, cf. Figs. 3 and 4) and allow the formation of the ternary sulfide.

3.4. Potential losses of elements during thermal treatments

Our previous studies [8] on the formation of $CuSbS_2$ via sulfurization of Cu–Sb metal precursors showed that evaporated Sb films, as well as converted $CuSbS_2$ films treated at 350 and 400 °C in excess sulfur vapour and under a N_2 flux of about 10 ml min^{-1}, show evidence of Sb depletion. Since the data reported by Piacente et al. [38] on the vapour pressure of Sb_2S_3 tends to exclude loss of substantial amounts of Sb in this temperature range by evaporation of Sb_2S_3 following decomposition of $CuSbS_2$, this phenomenon was attributed instead to a chemical vapour transport process caused by the excess sulfur [39] with the formation of an Sb-bearing volatile compound (such as Sb_2S_4, see below). Since the loss of Sb is clearly an issue for the achievement of good quality single-phase $CuSbS_2$ films, this aspect deserves further studies aimed at understanding (and controlling) the chemical equilibria behind it.

Similar problems in achieving single phase Cu_3BiS_3 films from metal precursors over a reasonably short sulfurization time are evident in the work of Gerein et al. [37]. In fact, it was reported that only crystalline Cu_2S (*Chalcocite*) was detected if Cu_3BiS_3 films were annealed in vacuum at high temperatures (600 °C), revealing the loss of Bi_2S_3 by thermal means. For this reason, the upper limit of the process temperature had to be restricted to 270 °C, imposing long processing times (>16 h) for sulfur uptake and complete conversion to be fully accomplished [10]. In order to avoid this, the same group has developed a one-step method for the synthesis of Cu_3BiS_3 thin films with good compositional and morphological properties, by reactive RF and DC sputter deposition of CuS and Bi on hot substrates [40,41]. Although this approach is appealing for its simplicity on a laboratory scale, its potential scale-up might pose technical and economical issues. In our previous studies [9] we observed no appreciable Bi depletion for converted films of Cu_3BiS_3 even at 550 °C in the time frame up to 16 h in the presence of an equivalent $S_{2(g)}$ partial pressure of 23 mbar. Therefore, we concluded that this pressure was sufficient to overcome the Bi losses via Le Chatelier effect on the decomposition equilibria of Cu_3BiS_3.

We now investigate the plausible decomposition reactions of the Sb and Bi sulfides in more detail from a thermochemical point of view. The review reported by Hua et al. [42] for their work on the volatilisation kinetics of Sb_2S_3 in steam atmosphere suggests that the Sb-S case is rather complex, with more than 22 species involved. Here the Sb-containing decomposing species considered is Sb_2S_3, as no thermochemical data are available for $CuSbS_2$. Although we are not dealing with $CuSbS_2$, the result can only be an overestimation of the losses, because $CuSbS_2$ is certainly more stable than Sb_2S_3 and Cu_2S [43], and even if this were not the case, Sb_2S_3 would likely be the ultimate result of the corresponding series of solid state decompositions (6).

$$(6)\quad 2CuSbS_{2(s)} \rightarrow Cu_2S_{(s)} + Sb_2S_{3(s)}$$

Similarly, the Bi-bearing decomposing species considered for Cu_3BiS_3 is Bi_2S_3, and the same considerations apply thereafter, as Bi_2S_3 would ultimately be the result of the solid state decomposition [44] (7).

$$(7)\quad 2Cu_3BiS_{3(s)} \rightarrow 3Cu_2S_{(s)} + Bi_2S_{3(s)}$$

The potential Sb- and Bi-bearing evolving species considered are those for which thermochemical data in the temperature range considered are available [22,45]: $Sb_{(g)}$, $Sb_{2(g)}$, $Sb_{4(g)}$, $SbS_{(g)}$, and $BiS_{(g)}$, $Bi_{2(g)}$ and $Bi_{(g)}$,with the following decomposition reactions (and equilibrium constants) investigated ((8)–(14)):

$$(8)\quad Sb_2S_{3(s)} \rightarrow 2Sb_{(g)} + 3/2S_{2(g)} \quad K_{P_{Sb}} = P^2_{Sb_{(g)}} \cdot P^{3/2}_{S_{2(g)}}$$

$$(9)\quad Sb_2S_{3(s)} \rightarrow Sb_{2(g)} + 3/2S_{2(g)} \quad K_{P_{Sb_2}} = P_{Sb_{2(g)}} \cdot P^{3/2}_{S_{2(g)}}$$

$$(10)\quad Sb_2S_{3(s)} \rightarrow 1/2Sb_{4(g)} + 3/2S_{2(g)} \quad K_{P_{Sb_4}} = P^{1/2}_{Sb_{4(g)}} \cdot P^{3/2}_{S_{2(g)}}$$

$$(11)\quad Sb_2S_{3(s)} \rightarrow 2SbS_{(g)} + 1/2S_{2(g)} \quad K_{P_{SbS}} = P^2_{SbS_{(g)}} \cdot P^{1/2}_{S_{2(g)}}$$

$$(12)\quad Bi_2S_{3(s)} \rightarrow 2BiS_{(g)} + 1/2S_{2(g)} \quad K_{P_{BiS}} = P^2_{BiS_{(g)}} \cdot P^{1/2}_{S_{2(g)}}$$

$$(13)\quad Bi_2S_{3(s)} \rightarrow 2Bi_{(g)} + 3/2S_{2(g)} \quad K_{P_{Bi}} = P^2_{Bi_{(g)}} \cdot P^{3/2}_{S_{2(g)}}$$

$$(14)\quad Bi_2S_{3(s)} \rightarrow Bi_{2(g)} + 3/2S_{2(g)} \quad K_{P_{Bi_2}} = P_{Bi_{2(g)}} \cdot P^{3/2}_{S_{2(g)}}$$

If the temperature dependence of the standard Gibbs free energies of the reactions ((8)–(14)) are known, given the known relationship between equilibrium constant and ΔG° (Eq. (5)), the

tendency of the Sb– and Bi–containing gaseous species to evolve from solid Sb_2S_3 and Bi_2S_3 can be expressed in terms of their equilibrium partial pressure as a function of the temperature and of the $S_{2(g)}$ partial pressure (Eqs. (6)–(12)).

$$\Delta G^{\circ} = -RT\ln(K_P) \tag{5}$$

$$P_{Sb_{(g)}} = e^{-(\Delta G^{\circ}/2RT)}/P_{S_{2(g)}}^{3/4} \tag{6}$$

$$P_{Sb_{2(g)}} = e^{-(\Delta G^{\circ}/RT)}/P_{S_{2(g)}}^{3/2} \tag{7}$$

$$P_{Sb_{4(g)}} = e^{-(2\Delta G^{\circ}/RT)}/P_{S_{2(g)}}^{3} \tag{8}$$

$$P_{SbS_{(g)}} = e^{-(\Delta G^{\circ}/2RT)}/P_{S_{2(g)}}^{1/4} \tag{9}$$

$$P_{BiS_{(g)}} = e^{-(\Delta G^{\circ}/2RT)}/P_{S_{2(g)}}^{1/4} \tag{10}$$

$$P_{Bi_{(g)}} = e^{-(\Delta G^{\circ}/2RT)}/P_{S_{2(g)}}^{3/4} \tag{11}$$

$$P_{Bi_{2(g)}} = e^{-(\Delta G^{\circ}/RT)}/P_{S_{2(g)}}^{3/2} \tag{12}$$

Figs. 6–7 show some graphical representations of the pressure equilibria for the Sb–S and Bi–S systems (Eqs. (6)–(9) and (10)–(12) respectively) as a function of temperature and $S_{2(g)}$ partial pressure.

In Figs. 6a–c and 7a–c the pressure equilibria functions of the Sb and Bi species respectively are cut by a "threshold pressure" plane (Eq. (13)) defined as the pressure limit above which the loss of Sb and Bi from films of $CuSbS_2$ and Cu_3BiS_3 1 μm thick exceeds 10% of the original content per cm^2 area of film and dm^3 capacity of sulfurization furnace (in static atmosphere conditions).

$$P^* = 10^{-8}\text{bar K}^{-1}\cdot T \tag{13}$$

In this way it is easy to identify the species that could potentially contribute mostly to the loss mechanisms and to pinpoint the sulfur pressure/temperature conditions for these processes to occur appreciably.

Fig. 6c can be divided into four regions. In region 1 the pressure of the Sb-bearing gaseous species is below the threshold pressure value. In region 2, $Sb_{4(g)}$ is the only species that shows a pressure exceeding the threshold value, while in region 3 and 4, $Sb_{2(g)}$ and $SbS_{(g)}$ also contribute progressively to the Sb depletion process. Careful inspection of Fig. 6b, also reveals that $Sb_{(g)}$ satisfies the threshold conditions at the very corner of minimum sulfur pressure and maximum temperature considered.

Fig. 6d shows the regions of the sulfur pressure/temperature diagram with different relative magnitude of the pressure for each volatile species, which is as follows.

Region 1: $SbS_{(g)} > Sb_{4(g)} > Sb_{(g)} > Sb_{2(g)}$
Region 2: $Sb_{4(g)} > SbS_{(g)} > Sb_{(g)} > Sb_{2(g)}$
Region 3: $Sb_{4(g)} > SbS_{(g)} > Sb_{2(g)} > Sb_{(g)}$

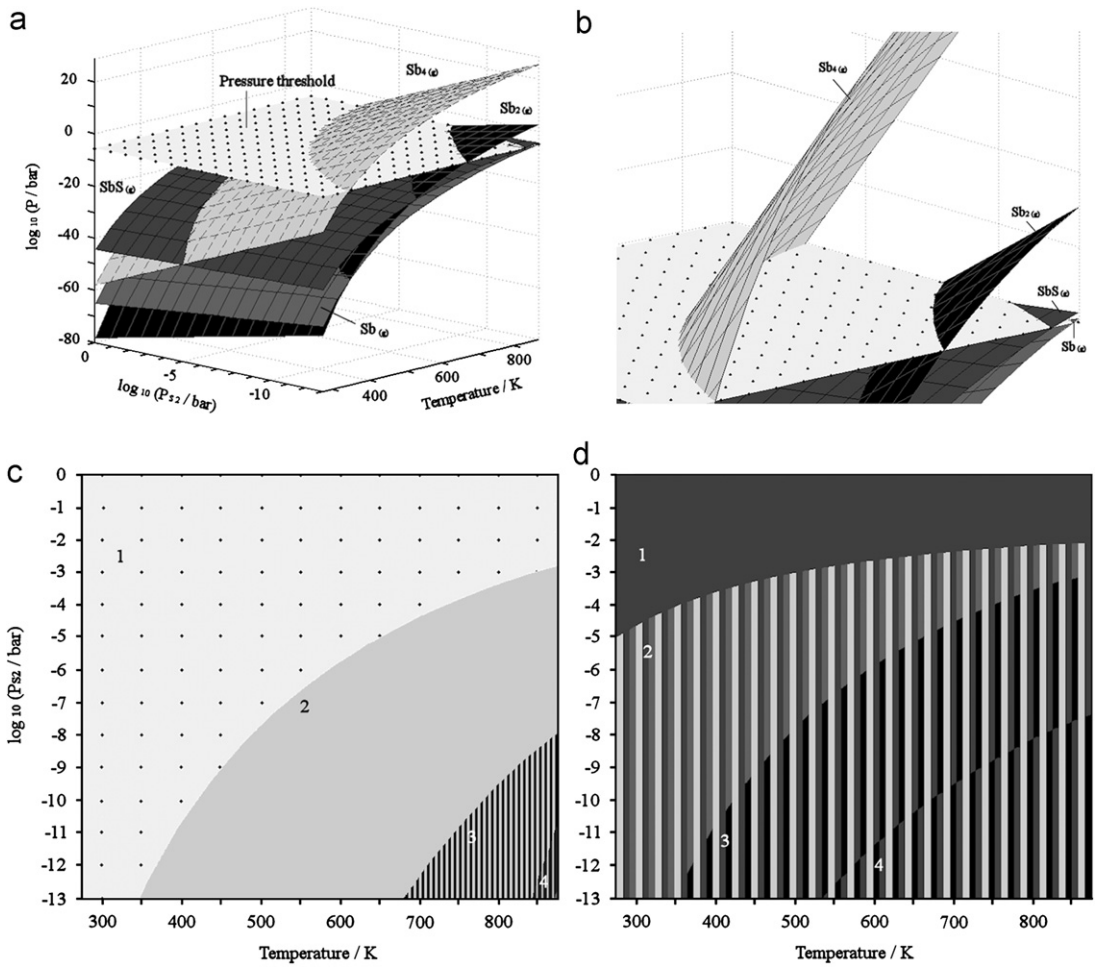

Fig. 6. 3D plot showing the pressures of $Sb_{(g)}$, $Sb_{2(g)}$, $Sb_{4(g)}$, and $SbS_{(g)}$ (Eqs. (6)–(9)) as a function of temperature and partial pressure of $S_{2(g)}$ in equilibrium with $Sb_2S_{3(s)}$, as per reactions ((8)–(11)) with the addition of the threshold pressure plane (Eq. (13)) (a–b). Intersection among the pressure equilibria functions of the Sb-bearing gaseous species (d) and of the latter with the threshold pressure plane (c) plotted as 2D projections of the 3D plot on the *x*–*y* plane.

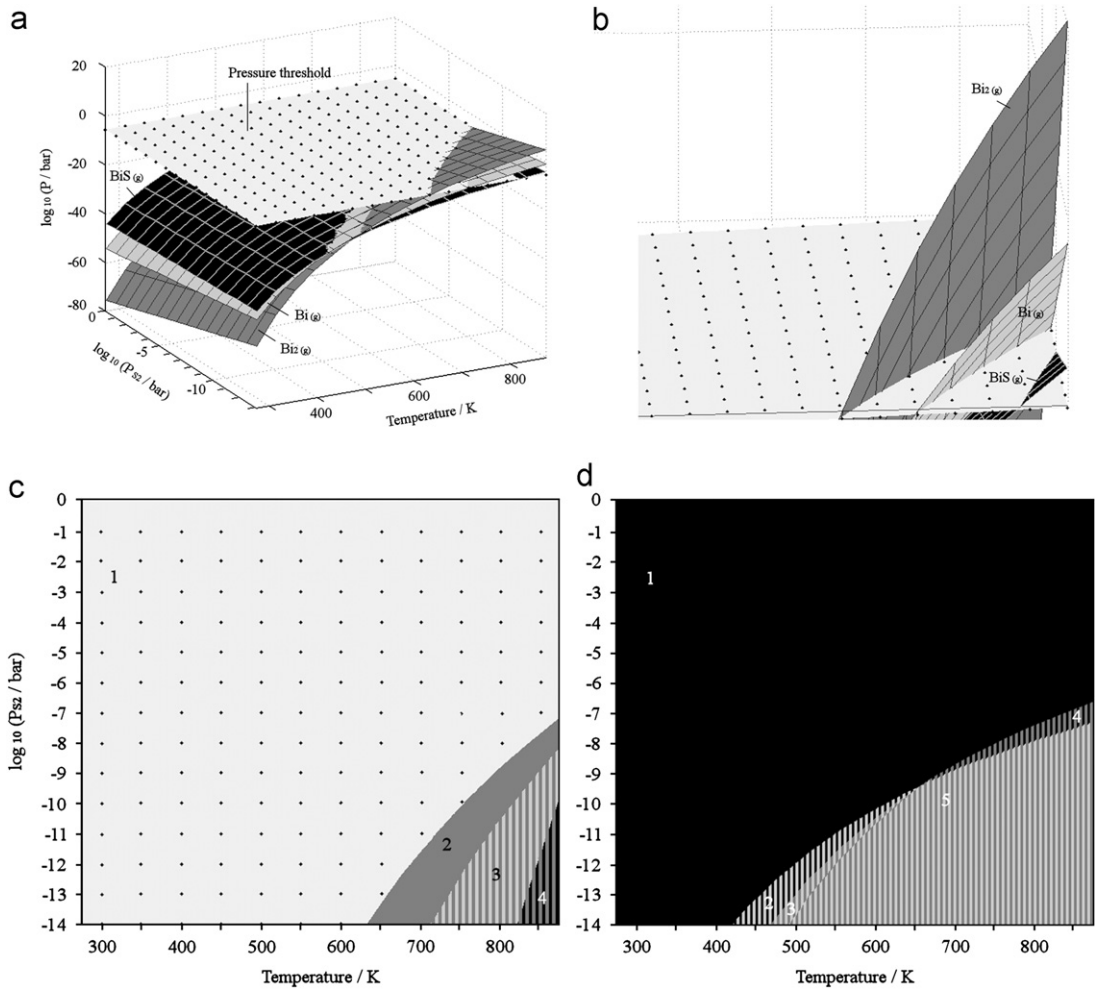

Fig. 7. 3D plot showing the pressures of $Bi_{(g)}$, $Bi_{2(g)}$, and $BiS_{(g)}$ (Eqs. (10)–(12)) as a function of temperature and partial pressure of $S_{2(g)}$ in equilibrium with $Bi_2S_{3(s)}$, as per reactions ((12)–(14)) with the addition of the threshold pressure plane (Eq. (13)) (a–b). Intersection among the pressure equilibria functions of the Sb-bearing gaseous species (d) and of the latter with the threshold pressure plane (c) plotted as 2D projections of the 3D plot on the *x*–*y* plane.

Region 4: $Sb_{4(g)} > Sb_{2(g)} > SbS_{(g)} > Sb_{(g)}$

The computation reveals that the decomposition reaction (10) with evolution of $Sb_{4(g)}$ and $3/2S_{2(g)}$ should be the major contributor to the Sb depletion in the $S_{2(g)}$ pressure/temperature range of our interest, despite mass spectrometric studies indicate $SbS_{(g)}$ as the dominant component of the vapour phase [46].

At 400 °C and 10^{-10} mbar of $S_{2(g)}$, an equilibrium partial pressure of $\sim 10^{-1}$ mbar can be estimated for the species $Sb_{4(g)}$ in contact with Sb_2S_3. With such a value we believe that a gas flux and/or a large volume of the furnace can easily lead to Sb losses via mass transport and saturation of the vessel, especially if prolonged dwell times are employed. However, from Fig. 6c is apparent that a $S_{2(g)}$ partial pressure of 0.1 mbar is sufficient to bring down the equilibrium pressures of the Sb-containing gas species to negligible values.

In our previous studies [8], a large excess of S was loaded into the furnace vessel, therefore the observed Sb losses cannot be attributed to reactions ((8)–(11)); an additional reaction must have occurred, one in which the sulfur takes part. A possibility might be given by the sulfur-rich molecule Sb_2S_4, which was suggested from mass spectrometric studies by Steblevskii et al. [47] to compose part of the vapour above Sb_2S_3 in the temperature range 377–467 °C. The amorphous nature of solid antimony thioantimonate (Sb_2S_4) suggests it may not result from elemental sulfur intercalation into the lattice of Sb_2S_3 [48] and it may actually exist as a molecular solid rather than an incommensurate species. It has been reported to undergo decomposition to solid Sb_2S_3 and sulfur in the temperature range 200–400 °C, which is also why it is used as a solid lubricant [49]. However, the reverse reaction would be plausible (15):

(15) $Sb_2S_{3(s)} + 1/2S_{2(g)} \rightarrow Sb_2S_{4(g)}$

where mass transport via gaseous phase in excess sulfur is a possibility. Depending on the sign of the enthalpy of reaction, the gas molecule Sb_2S_4 will then incur decomposition back to $Sb_2S_{3(s)} + S_{2(g)}$ in the hotter or colder parts of the furnace. Indeed, Steblevskii et al. [50] suggest that the formation of $Sb_2S_{4(g)}$ occurs via the reaction of $S_{2(g)}$ with gaseous molecular Sb_2S_3.

As for the Sb case, Fig. 7c can be divided into four regions. In region 1 the pressure of the Bi-bearing gaseous species is below the threshold pressure value. In region 2, $Bi_{2(g)}$ is the only species that shows a pressure exceeding the threshold value, while in region 3 and 4, $Bi_{(g)}$ and $BiS_{(g)}$ contribute progressively to the Bi depletion process, as can be also inferred from Fig. 7b.

Fig. 7d shows the regions of the sulfur pressure/temperature diagram with different relative magnitudes of the pressures for each volatile species, which are as follows.

Region 1: $BiS_{(g)} > Bi_{(g)} > Bi_{2(g)}$
Region 2: $Bi_{(g)} > BiS_{(g)} > Bi_{2(g)}$
Region 3: $Bi_{(g)} > Bi_{2(g)} > BiS_{(g)}$

Region 4: $Bi_{2(g)} > BiS_{(g)} > Bi_{(g)}$
Region 5: $Bi_{2(g)} > Bi_{(g)} > BiS_{(g)}$

From Fig. 7 it seems clear that the species that has the potential to contribute most to depletion of Bi at high temperature from solid Bi_2S_3 (i.e. also from solid Cu_3BiS_3) is $Bi_{2(g)}$ through reaction (14). This process might indeed explain the Bi losses observed by Gerein et al. [37] on the Cu_3BiS_3 films annealed in vacuum at 600 °C.

4. Concluding remarks and future work

In principle, any two-stage process consisting of precursor film conversion by mass transfer from a gas or liquid phase followed by solid state reaction is subject to phase segregation. This is an intrinsic process flaw that becomes more important, as the complexity of the system considered increases [51]. Nevertheless, the simplicity of such a process makes it a readily scalable alternative to more complicated routes, although the minimisation of secondary phase segregation is a strict requirement for its successful application.

With the processing conditions investigated in the present work, the formation of thin films of $CuSbS_2$ and Cu_3BiS_3 by conversion of the corresponding metal precursors in the presence of elemental sulfur vapour occurs via formation of the binary sulfides and their subsequent solid state reaction.

A Time Temperature Reaction diagram for the conversion of Cu–Bi precursor films into Cu_3BiS_3 was created with an RTP approach by analysis of the ex-situ X-ray diffractograms. Kinetic information was extracted from the temperature dependence of the time required for the ternary sulfide to emerge and form completely. The findings indicate that the activation energy for the formation of Cu_3BiS_3 by diffusion across the CuS–Bi_2S_3 interface is considerably higher than the one required for $CuSbS_2$ to form out of the Cu_2S–Sb_2S_3 bulk diffusion couple. This result is consistent with an expected more sluggish diffusion of Bi as opposed to Sb, given the larger atomic radius of the former.

It seems clear that the initial process conditions have a strong effect on the growth of the secondary phases and their subsequent physical displacement, which in turn has shown to influence the morphology of the final compound film. If this phenomenon cannot be avoided, it might be possible to minimise its effects by fine-tuning of the chalcogenisation conditions.

For example, excellent results were obtained on CIGS by Merdes et al. [52] with a rapid thermal process, where the temperature profile and sulfur partial pressure were carefully adjusted so as to improve the reaction progress. Furthermore, a very recent paper by Maeda et al. [53] shows how the morphology of CZTS films obtained by sulfurization of metal precursors is improved if a low concentration (3%) of H_2S is employed, and how this enhances the photoactive properties of the layers, due to an increase of the short circuit current.

In the present case, despite the thermodynamics of sulfide formation, the reactivity of Cu towards elemental sulfur vapour was found to be much higher than that of Sb and Bi. This difference is thought to be the main cause of the prominent phase segregation of CuS observed for both Cu–Sb and Cu–Bi systems. The different kinetics was attributed to a different mechanism of sulfide growth, in accordance to a series of modified Pilling Bedworth coefficients calculated for the Cu/CuS, Sb/Sb_2S_3, and Bi/Bi_2S_3 interfaces.

A lower reactivity of the sulfurizing atmosphere is likely to reduce the sulfide nucleation rate and slow down the sulfur uptake of the metal precursor, leading to a less segregated (even amorphous) intermediate film [37]. It might be possible to achieve this, either by replacing sulfur with hydrogen sulfide or by reducing its partial pressure.

The characteristic porosity of the Cu–Bi co-electroplated precursors might make them ideal for a sulfurization with H_2S at temperature lower than 270 °C. The high surface area would possibly increase the reactivity of Bi allowing its conversion to Bi_2S_3 to occur over a similar timeframe of the corresponding of Cu, thus reducing Bi coalescence and segregation.

A subsequent annealing stage at higher temperature would promote the diffusion of the binary sulfides and likely enhance the crystallinity of the films.

Thermochemical analysis of the potential Sb and Bi losses suggests that such second annealing stages should be performed in the presence of a moderate background pressure of elemental sulfur vapour, so that the corresponding reactions ((8)–(14)) are prevented due to the mass equilibrium effect. However, special attention must be given to the annealing of $CuSbS_2$, because in this case an additional mechanism of elemental depletion appears to operate in which excess sulfur might have the opposite effect. Further studies are still required to clarify this aspect.

Acknowledgments

Kieran Molloy, Aron Walsh, Jesse Dufton, Pooja Panchmatia and Charles Cummings (University of Bath – Chemistry Department) are gratefully acknowledged for the constructive discussions about this work.

Fulvio Pinto, Francesco Ciampa (University of Bath – Mechanical Engineering Department) and Ettore Barbieri (University of Oxford) are acknowledged for their help in computing the Sb–S and Bi–S pressure equilibria with the MATLAB software.

The Mo coated SLG substrates were kindly provided by Stefan Schäfer (Enthone GmbH) and Guillaume Zoppi (Northumbria University).

Alan Dinsdale is acknowledged for the adapted Cu–Bi phase diagram depicted in Fig. 4 which was predicted using MTDATA, software from the National Physical Laboratory for the calculation of phase equilibria from thermodynamic data [19] (original data taken from [20]).

Funding was provided by EPSRC.

Appendix A. Supplementary materials

Supplementary data associated with this article can be found in the online version at doi:10.1016/j.jssc.2011.11.025.

References

[1] H.S. Ulal, B. von Roedern, Solid State Technology 51 (2008) 52–54.
[2] N.G. Dhere, Solar Energy Materials and Solar Cells 91 (2007) 1376–1382.
[3] H. Katagiri, K. Jimbo, W.S. Maw, K. Oishi, M. Yamazaki, H. Araki, A. Takeuchi, Thin Solid Films 517 (2009) 2455–2460.
[4] B.H. Ryu, S.P. Yoon, J. Han, S.W. Nam, T.H. Lim, S.A. Hong, K.B. Kim, Electrochimica Acta 50 (2004) 189–198.
[5] E. Antolini, Solid State Ionics 170 (2004) 159–171.
[6] K.N. Lee, in: R. Dennis (Ed.), The Gas Turbine Handbook, U.S. Department of Energy, National Energy Technology Laboratory, Morgantown - West Virginia, 2006.
[7] B.J. Stanbery, Critical Reviews in Solid State & Materials Science 27 (2002) 73.
[8] D. Colombara, L.M. Peter, K.D. Rogers, J.D. Painter, S. Roncallo, Thin Solid Films 519 (2011) 7438–7443.
[9] D. Colombara, L.M. Peter, K. Hutchings, K.D. Rogers, S. Schäfer, J.T. Dufton. Formation of Cu_3BiS_3 thin films via sulfurization of Bi-Cu metal precursors, Journal of Thin Solid Films, in preparation.
[10] N.J. Gerein, J.A. Haber, Chemistry of Materials 18 (2006) 6289–6296.
[11] V.F. Ross, Economic Geology 49 (1954) 734–752.
[12] G. Tammann, Zeitschrift Für Anorganische und Allgemeine Chemie 111 (1920) 78.
[13] H. Schmalzried, Angewandte Chemie International Edition in English 2 (1963) 251–254.

[14] V. Kupčík, L. Veselá-Nováková, Mineralogy and Petrology 14 (1970) 55–59.
[15] L.F. Lundegaard, E. Makovicky, T. Boffa-Ballaran, T. Balic-Zunic, Physics and Chemistry of Minerals 32 (2005) 578–584.
[16] L.F. Lundegaard, R. Miletich, T. Balic-Zunic, E. Makovicky, Physics and Chemistry of Minerals 30 (2003) 463–468.
[17] L.H. Ahrens, Geochimica et Cosmochimica Acta 2 (1952) 155–169.
[18] R. Shannon, Acta Crystallographica Section A 32 (1976) 751–767.
[19] R.H. Davies, A.T. Dinsdale, J.A. Gisby, J.A.J. Robinson, S.M. Martin, Calphad 26 (2002) 229–271.
[20] A.T. Dinsdale, A. Watson, A. Kroupa, J. Vrestal, A. Zemanova, J. Vizdal, Lead-Free Solders Volume 1. COST office, 2008.
[21] D. Chakrabarti, D. Laughlin, Journal of Phase Equilibria 5 (1984) 148–155.
[22] O. Knacke, O. Kubaschewski, Thermochemical Properties of Inorganic Substances, 2nd ed., Springer-Verlag, Verlag Stahleisen Berlin, New York, Düsseldorf, 1991.
[23] D.M. Berg, A. Redinger, P.J. Dale, S. Siebentritt, Journal of the American Chemical Society (2011) null-null.
[24] J.J. Scragg, P.J. Dale, L.M. Peter, Thin Solid Films 517 (2009) 2481–2484.
[25] C.H. Tsai, J.M. Ting, W.H. Ho, Thin Solid Films 517 (2009) 4731–4734.
[26] C. Broussillou, G. Savidand, L. Parissi, J.S. Jaime-Ferrer, P.P. Grand, C. Hubert, O. Roussel, E. Saucedo, V. Bermudez, M. Andrieux, M.H. Berger, M. Jeandin, Energy Procedia 2 (2010) 9–17.
[27] L.M. Peter, Journal of Electroanalytical Chemistry and Interfacial Electrochemistry 98 (1979) 49–58.
[28] Z. Grubać, M. Metikos-Hukovic, Thin Solid Films 413 (2002) 248–256.
[29] N.B. Pilling, R.E. Bedworth, Journal of the Institute of Metals 29 (1923) 529–591.
[30] S. Sanchez, S. Cassaignon, J. Vedel, H.G. Meier, Electrochimica Acta 41 (1996) 1331–1339.
[31] S. Cassaignon, T. Pauporté, J. Guillemoles, J. Vedel, Ionics 4 (1998) 364–371.
[32] J.F. Nowak, M. Lambertin, J.C. Colson, Corrosion Science 17 (1977) 603–613.
[33] J. Furer, M. Lambertin, J.C. Colson, Corrosion Science 17 (1977) 625–632.
[34] A. Etienne, Journal of The Electrochemical Society 117 (1970) 870–874.
[35] N.R. de Tacconi, K. Rajeshwar, R.O. Lezna, The Journal of Physical Chemistry 100 (1996) 18234–18239.
[36] Z. Grubać, M. Metikos-Hukovic, Journal of Electroanalytical Chemistry 565 (2004) 85–94.
[37] N.J. Gerein, (2005).
[38] V. Piacente, P. Scardala, D. Ferro, Journal of Alloys and Compounds 178 (1992) 101–115.
[39] J. Yang, Y.C. Liu, H.M. Lin, C.C. Chen, Advanced Materials 16 (2004) 713–716.
[40] N.J. Gerein, (2006).
[41] N.J. Gerein, J.A. Haber, Chemistry of Materials 18 (2006) 6297–6302.
[42] Y. Hua, Y. Yang, F. Zhu, Journal of Materials Science and Technology 19 (2003) 4.
[43] A. Sugaki, H. Shima, A. Kitakaze, Technology reports, Technology reports of Yamaguchi University, 1973, pp. 169–181.
[44] A. Sugaki, H. Shima, Technology reports, Technology report of Yamaguchi University, 1972, pp. 45–70.
[45] P.C. Chaubal, M. Nagamori, Metallurgical and Materials Transactions B 19 B (1988) 547–556.
[46] V.P. Zakaznova-Iakovleva, A.A. Migdisov, V.P. Zakaznova-Iakovlevaa, O.M. Suleimenov, A.E. Williams-Jones, Y.V. Alekhin, Geochimica et Cosmochimica Acta 65 (2001) 289–298.
[47] A.V. Steblevskii, V.V. Zharov, A.S. Alikhanyan, V.I. Gorgoraki, A.S. Pashinkin, Russian Journal of Inorganic Chemistry 34 (1989) 891–894.
[48] J.P. King, Y. Asmeron, Tribology Transactions (1981) 497–504.
[49] D. Ozimina, Tribology Letters 13 (2002) 111–117.
[50] A.V. Steblevskii, V.V. Zharov, A.S. Alikhanyan, A.S. Pashinkin, V.I. Gorgoraki, Russian Journal of Inorganic Chemistry 34 (1989) 1821–1826.
[51] A. Ennaoui, M. Lux-Steiner, A. Weber, D. Abou-Ras, I. Kötschau, H.W. Schock, R. Schurr, A. Hölzing, S. Jost, R. Hock, T. Voß, J. Schulze, A. Kirbs, Thin Solid Films 517 (2009) 2511–2514.
[52] S. Merdes, R. Mainz, J. Klaer, A. Meeder, H. Rodriguez-Alvarez, H.W. Schock, M.C. Lux-Steiner, R. Klenk, Solar Energy Materials and Solar Cells 95 (2011) 864–869.
[53] K. Maeda, K. Tanaka, Y. Fukui, H. Uchiki, Solar Energy Materials and Solar Cells 95 (2011) 2855–2860.